International Journal Of Industrial Electronics Control and Optimization (IECO)
Print ISSN: 3517-2645
Online ISSN: 3568-2645
Homepage: https://ieco.usb.ac.ir/

Tuning Spring Constant of a Beam for a Promising Reduction in the Actuation Voltage of a V-Band RF MEMS Switch

Farid Khamouei Touli[1], Javad Yavand Hasani[2]

School of Electrical Engineering, Iran University of Science and Technology,Tehran, Iran[1,2]
Corresponding author's email: yavand@iust.ac.ir

Article Info

Article type:
Research Article

Article history:
Received: 28-Dec-2023
Received in revised form: 6-March-2024
Accepted: 11-March-2024
Published online: 21-June-2024

Keywords:
Actuation Voltage,
Modified Energy Method,
RF-MEMS,
Switching Time,
Von Mises Stress.

ABSTRACT

Radiofrequency microelectromechanical system (RF-MEMS) switches are utilized across a broad spectrum of industries, including telecommunications, aerospace, defense, and smartphone technology.Herein, we proposed a new numerical and simulation analysis approach for spring constant (k) values as the characteristic mechanical parameters of RF MEMSs using the modified energy method (MEM). The proposed RF-MEMS switch was analyzed and simulated using the COMSOL package, and the findings confirmed that the alteration in the position and length (L) of the beams not only diminishes k significantly but also provides actuation-voltage VAC ultrasensitive structures and great concomitance between numerical and simulation k and VAC values. VAC value for the L-dependent numerical k (0.07 N m^{-1}) was calculated to be 1.61 V which was validated with simulation outputs at 0.08 N m^{-1} and 1.80 V for k and VAC, respectively. Additionally, the switching time (ts), Von Mises Stress (VMS), natural frequency (fn) and mass (m) characteristic mechanical parameters were found to be 25.60 µs, 4.50 MPa, 3118.60 Hz , and0.21 ng, respectively. RF analysis was conducted in HFSS, revealing promising simulation results for the studied RF-MEMS switches. The return loss demonstrates excellent performance, registering better than -1 dB at 46 GHz. Furthermore, the insertion loss is noteworthy, exceeding expectations with values better than -0.7 dB at 46 GHz. Importantly, the isolation is impressive, exceeding -25 dB across the frequency range from 40 GHz to 35 GHz, all achieved with a modest actuation voltage of 1.8 V. This study contributes valuable insights intothe design and application of low-actuation-voltage RF-MEMS switches.

NOMENCLATURE

$RFMEMS$	Radiofrequency micro Electromechanical system	f_n	Natural frequency
k	Spring constant	MEM	Modified energy method
V_{AC}	Actuation voltage	t_s	Switching time
m	Mass	VMS	Von Mises Stress

Copyright © F. Khamouei Touli and J.Yavand Hasani.
Publisher: University of Sistan and Baluchestan

I. Introduction

In the pathway of the evolution of electrostatic switches, the paradigm of recent research has focused on improving structural challenges of field-effect transistors (FETs) and positive-intrinsic-negative (PIN) diodes which consist of excessive power consumption, high rate of return loss, low isolation,and limited bandwidth [1]. Microelectromechanical systems (MEMSs) as one of the most promising candidates which represented versatile properties such as superior isolation sensitivity and limited return loss have been interested in recent years. Several capacitors, switches, and phase shifters are benefited from MEMSs for wide irreplaceable applications including automatic test equipment, advanced communication technology, satellite communications, aerospace, defence, and smartphones [2, 3]. The MEMSs work based on electrostatic, magnetic, and piezoelectric actuators to provide the demand energy for the mechanical movement of these pieces [4]. Among the array of actuation methods, electrostatic actuation has emerged as the most efficient. popular method of switch actuation due to its high speed, easier construction, as well as tuneable size, high reliability and stability against environmental and temperature changes, satisfactory power consumption, high scalability, more straightforward structure and compatibility with CMOS technology [5]. The most important challenge in RF-MEMS switches is its limitation in accessingthe low actuation voltage (V_{AC}) synchronous with switch low input loss. Additionally, by decreasing V_{AC}, the air gap width is reduced in switch structure and leads to insertion loss increases. Some versatile methods such as increasing the section level, reducing the gap between the switch beam and the down electrode, and structure design with a low spring constant have been applied to reduce the V_{AC} in the RF-MEMS switches structures [6]. Amongst, increasing the section level and gap reduction between the beam and the down electrode to lead to theuntenability of the switch size and insertion loss, respectively [7]. Therefore, V_{AC} reduction is a promising and superior method than other approaches for designing a structure with low spring constant [8, 9]. In this regard, Sharma *et al*. decrease the spring constant by a new structure with non-uniform spiral curves and variable curve width which the obtained values for V_{AC} were between 15 to 3 V and for curve width was 100 µm to 280 µm. Additionally, MEM was applied to obtain displacement and eventually spring constant [10]. Ganji *et al.* report a new small area structure for RF-MEMS series switches by obtaining accurate spring constant and V_{AC} (4.05 V) [11]. In another study, Guha *et al.* applied capacitor analysis to the calculation of the electrostatic power effects and marginal fields and an authentic relationship was achieved; as well as a suitable algorithm was reported to improve the effectiveness of the hole which the proposed structure successfully decreases V_{AC} to 2.1 V [12].

In this study, we proposed a new numerical and simulation analysisapproach for spring constant (*k*) values as the characteristic mechanical parameter for highly flexible RF-MEMSs constructed from gold (Au) and silicon nitride (Si_3N_4) using the modified energy method (MEM). The as-proposed RF-MEMS switch was analyzed and simulated in the COMSOL package.

II. Methodology

A. Understudy switch structure

The as- designed RF-MEMS switch was developed based on the previous report by Guha *et al.* with a changing its square wave shape serpentine to non-uniform serpentine flexure with a two-meander section divided into seven beams Fig . 1(a) [13, 14]. In the suggested structure, there are four horizontal beams with length *a*, and three vertical beams L_i, Fig . 1(b).

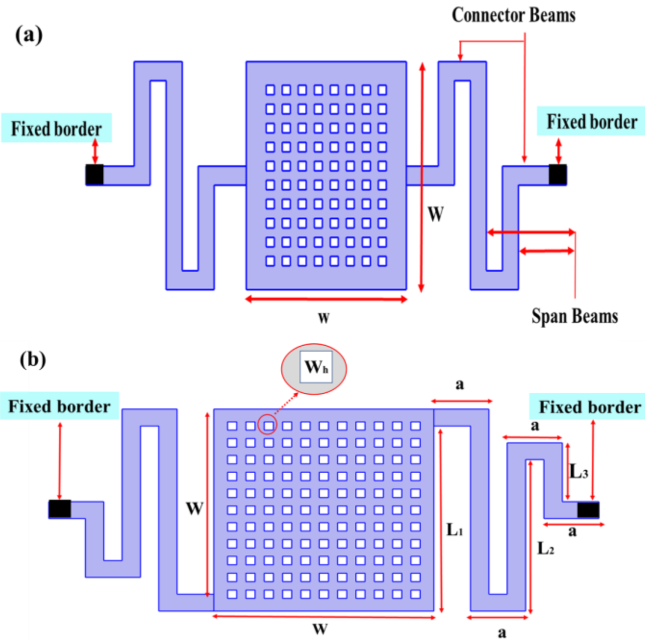

Fig. 1. The structure of the RF-MEMS switch by Guha *et al.* [14] (a); Proposed structure in this study (b)

The size of different sections of the suggested switch was summarized in Table 1. The RF-MEMS structure underwent optimization, and an analysis of its mechanical characteristics was conducted.The switch process is presented as follows: the bridge material is selected by considering Young's modulus and mass density so that Young's modulus has to be more than mass density by a selection of gold as a bridge. The Si_3N_4 and SiO_2 with a dielectric constant of 7.6 and 3.6, respectively were selected for the desirable comparison as dielectric materials by investigation of dielectric constant, dielectric resistance, leakage current, and surface roughness characters [15].

B. Mathematical models for the suggested structure

The modified energy method (MEM) was applied to analyse the spring constant of the proposed structure. First, the beam displacement was calculated based on the electrostatic force, and

then the spring constant was calculated by Eq. 1 [16].

$$k_z = \frac{F_z}{\delta_z} \quad (1)$$

Where F_z is the exerted electrostatic force, and δ_z is the displacement of the beam. As in a static problem, it is supposed that the structure is perfectly balanced, hence, it is supposed that the sum of all internal and external forces (F), as well as the sum of all bending (M) and torsional (T) moments, are zero.Eq. 2 shows this supposition [16].

$$\sum T = 0,\ \sum M = 0,\ \sum F = 0 \quad (2)$$

In Fig .Fig . 2(a), in order to obtain static balance and to obtain bending and torsional anchors in different parts of the beam, the whole structure is assumed as a support as well as a sliding surface.

TABLE 1: SUGGESTED STRUCTURE CHARACTERISTICS

Parameter	Symbol	Size (µm)
Bridge width	w	120
Bridge length	W	120
Horizontal beams length	a	30
Vertical beam length	L1	110
Second vertical beam length	L2	90
Third vertical beam length	L3	30
Curve width	w_m	10
Dielectric thickness	td	0.15
Mobile bridge thickness	tb	0.60
Ari distance between two surfaces	g_0	2.50
Holes length size	w_h	5.0
Holes number	$n_l .n_w$	11*11
Dielectric constant	ε_r	7.60
Gold Young’s modulus	E	79GPa

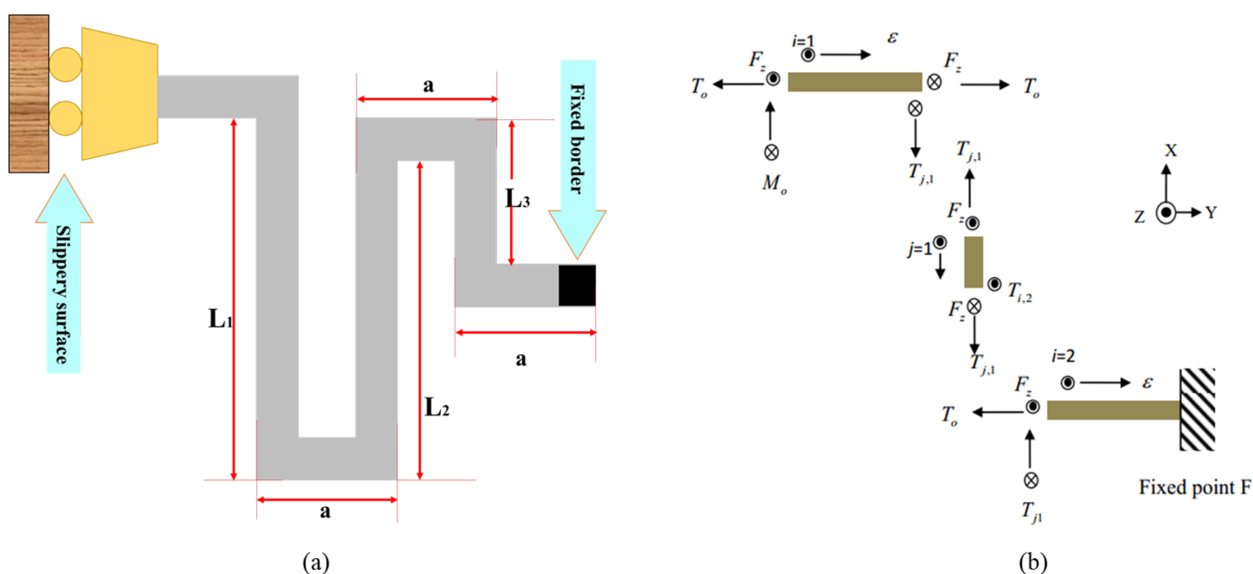

Fig. 2. Characteristics of curve spiral sections for solving a static problem (a); Analysis of the suggested structures with different curves and their sections (b) [10].

Fig . 2(b) shows forces and moments decomposition in various parts of the beam. Furthermore, to make the structure remain static, M_0 and T_0 were suspended in the opposite direction of the constant head on the bridge side. The analysis begins withthe suspended part and moves to the T constant, finally M is calculated for each part of the beam considering the balance condition according to the related equations summarized in Table 2. Electrostatic force in RF-MEMS parallel capacitor switches is applied to change the switch condition from upstate to downstate. Therefore, it is possible to consider this force in line with the Z-axis. Using the Castiglione theorem, to simplify this problem, it is supposed that no other force in

no other direction is exerted on beams. In the MEM, the energy and spring constant were calculated from external force and internal moments according to Eq. 3. Hence, it is possible to define displacement as in Eq. 4 [16, 17].

$$U=\begin{pmatrix}\sum_{i=1}^{N}\int_{0}^{a}\left(\frac{M_{a,i}^{2}}{2EI_{x,a}}+\frac{T_{a,i}^{2}}{2GJ_{a}}\right)d\varepsilon+\\ \sum_{j=1}^{N}\int_{0}^{Lj}\left(\frac{M_{b,j}^{2}}{2EI_{x,b}}+\frac{T_{b,j}^{2}}{2GJ_{b}}\right)d\varepsilon\end{pmatrix} \quad (3)$$

$$\delta_z=\frac{\partial U}{\partial F_z} \quad (4)$$

where E is Young's modulus, G is thetorsional moment modulus, J is torsion constant, as well as I_{xa} and I_{xb} are the moment of inertia for vertical and horizontal curves whose values are calculated by Eq. 5 [16].

$$I_x=I_{x,a}=I_{x,b}=\int_{-w/2}^{w/2}\int_{-t/2}^{t/2}x^2dxdz=\frac{wt^3}{12} \quad (5)$$

The moment of inertia in line with z is as in Eq. 6 [16].

$$I_z=\int_{-t/2}^{t/2}\int_{-w/2}^{w/2}x^2dxdz=\frac{tw^3}{12} \quad (6)$$

Torsion modulus is defined in Eq. 7 [16].

$$G=\frac{E}{2(1+V)} \quad (7)$$

Where E is Young's modulus, and V is Poisson's ratio. The torsion constant was calculated according to the moment of inertia relation torsion constant for vertical and horizontal curves in the rectangular bridge, as Eq. 8 [16].

$$J=0.413(I_X+I_Z) \quad (8)$$

In the fixed-head state energy change to bending moment (θ_0) and energy change to torsional moment ($\emptyset_0$) were calculated as follows:

$$\theta_0=\frac{\partial U}{\partial M_0}=0 \qquad \emptyset_0=\frac{\partial U}{\partial T_0}=0 \quad (9)$$

In simple terms, the slope is zero in the fixed head for bending and torsional movements. To solve the problem, first, bending and torsional moments must be calculated in the fixed head. Therefore, $\theta_0=0$ and $\emptyset_0=0$ wereassumed for borders that [16].

TABLE 2: ANALYZING MOMENTS FOR DIFFERENT SECTIONS OF THE CURVE IN THE SUGGESTED STRUTURE

Vertical beam		Horizontal beam	
Torsional moment	**Bending moment**	**Torsional moment**	**Bending moment**
$T_{b1}=M_0-F_za$	$M_{b1}=-T_0-F_zx$	$T_{a1}=T_0$	$M_{a,1}=-M_0-F_zx$
$T_{b2}=M_0+2f_za$	$M_{b2}=-F_zx-T_0-F_zL_1$	$T_{a2}=T_0-F_zL_1$	$M_{a2}=-F_za-F_zx-M_0$
$T_{b3}=M_0-3aF_z$	$M_{b3}=-T_0-F_zx+F_z(L_1-L_2)$	$T_{a3}=T_0-F_z(L_1-L_2)$	$M_{a3}=M_0-F_z(2a)-F_zx$
0	0	$T_{a4}=T_0+F_z(L_1-L_2+L_3)$	$M_{a4}=M_0-3F_za-f_zx$

$$\theta_0=\frac{\partial U}{\partial M_0}=\begin{pmatrix}\sum_{i=1}^{2N}\int_{0}^{a}\left(\frac{M_{a,i}}{EI_{x,a}}\frac{\partial M_{a,i}}{\partial M_0}+\frac{T_{a,i}}{GJ_{a}}\frac{\partial T_{a,i}}{\partial M_0}\right)d\varepsilon+\\ \sum_{j=1}^{2N}\int_{0}^{Lj}\left(\frac{M_{b,j}}{EI_{x,b}}\frac{\partial M_{b,j}}{\partial M_0}+\frac{T_{b,j}}{GJ_{b}}\frac{\partial T_{b,j}}{\partial M_0}\right)d\varepsilon\end{pmatrix} \quad (10)$$

$$\emptyset_0=\frac{\partial U}{\partial T_0}=\begin{pmatrix}\sum_{i=1}^{2N}\int_{0}^{a}\left(\frac{M_{a,i}}{EI_{x,a}}\frac{\partial M_{a,i}}{\partial T_0}+\frac{T_{a,i}}{GJ_{a}}\frac{\partial T_{a,i}}{\partial T_0}\right)d\varepsilon+\\ \sum_{j=1}^{2N}\int_{0}^{Lj}\left(\frac{M_{b,j}}{EI_{x,b}}\frac{\partial M_{b,j}}{\partial T_0}+\frac{T_{bj}}{GJ_{b}}\frac{\partial T_{b,j}}{\partial T_0}\right)d\varepsilon\end{pmatrix} \quad (11)$$

Solving the above equations resulted inthe values of the M_0 and T_0 (based on the size of vertical and horizontal beams) as well as G, I, and F. Moreover, as F_z had to be derived to obtain the displacement, M_0 and T_0 are written as C_1F_z and C_2F_z.

$$M_0=f(a, L_1, L_2, L_3, G, I, F_z)=C_1F_z \quad (12)$$

$$T_0=f(a, L_1, L_2, L_3, G, I, F_z)=C_2F_z \quad (13)$$

Substituting the values for the parameters listed in Table 2 into Eq .12 and 13 yields the values of M_0 and T_0. Since the problem is parametric, MATLAB is utilized to symbolically solve the problem due to the complexity and length of the equations. Considering the size of different sections of the suggested structure in Table 1 the value of the spring constant was calculated. To investigate the spring constant of vertical and horizontal sections, the vertical and horizontal are scanned separately from 20 µm to 250 µm.

C. V_{AC} Analysis for the Suggested Switch

The most important challenge in RF-MEMS switches is its limitation to access to the low V_{AC} synchronous with switch low input loss. RF MEMS switch dynamic Eq. 14 is as follows [2].

$$m\frac{d^2x}{dt^2}+b\frac{dx}{dt}+kx=\frac{\varepsilon_0AV^2}{2\left(d-x+\frac{t_d}{\varepsilon_r}\right)} \quad (14)$$

Where m is switch mass, b is thedamping coefficient resulting from fluid viscosity, and k is theswitch spring constant. The right side of the equation represents the electrostatic power equation. Solving Eq. 14 yields the V_{AC} [2, 8].

There are three possible ways to decrease the actuation voltage:

- Increasing section level, which also increases switch size and insertion loss.
- Gap reduction between switch bar and low electrode, which is practically accompanied by problems like insertion loss increase.
- Structure design with low spring constant.

$$V_{AC} = \sqrt{\frac{8kg_0^3}{27A\varepsilon_0}} \quad (15)$$

As in Eq.15, V_{AC} depends on three factors includingspring constant, actuation surface size,and air distance. Change in any of these factors affects the V_{AC}. Applying the results of the last section, an analytical equation for actuation voltage can be derived that can be obtained by replacing the results of Eq. 1 in Eq. 15. Due to the equation length, the V_{AC} is analyzed in MATLAB software.

III. Suggested Simulation Structure, Results and Discussions

This section presents the results obtained from the mechanical structure simulation using COMSOL software, including the V_{AC}, switching time, natural frequencies, and the designed switch mass, as well as the Von Mises stress for the proposed structure.

A. Effect of vertical and horizontal sections of the beam on the spring constant and V_{AC}

Vertical and horizontal sections are important operational variable for optimizing the spring constant and V_{AC} which they were studied in the range of 20 µm to 250 µm. Results revealed that the increase in horizontal beams than that of vertical beams has superior effects on constant spring reduction which is comfortable with theMEM method (see Fig . 3(a)). By increasing the vertical beam from 20 µm to 100 µm spring constant was reduced from 0.17 N m^{-1} to 0.002 N m^{-1}. At first sight, it might seem useful in achieving our goal, but in the structure design, drag force in returning the switch to the initial state and consumption level values haveto be considered. In the range of 20 µm to 250 µm Vertical sections have fewer changes than horizontal beams. Scanning vertical beams changed the spring constant to approximately 0.02 N m^{-1}. The effect of different sections of the suggested structure on V_{AC} is shown in Fig . 3(b). It can be seen that by decreasing the horizontal beam, V_{AC} decreases with a steep slope. Changing the horizontal section from 20 µm to 100 µm the V_{AC} reduces from 2.5 V to 0.25 V. Vertical beams influence the V_{AC} less as compared to horizontal beams, and by increasing the beams from 20 µm to 250 µm, the actuation voltage changes from 1.6 V to 1.4 V. Table 3 summarizes the size change in horizontal and vertical beams as well as the effect of this change on spring constant and V_{AC}. Reducing air distance is another method to reduce voltage. Table (4) shows actuation voltage values for different air distances. The V_{AC} for a2.5 µm air distance is 1.6107 V. Air distance has to be selected such that the construction phase of the suggested structure is smoothly handled. Therefore, 2.5 µm air distance is selected to prevent any problems [2]. According to Table 4, when lower air distances are selected, lower V_{AC} is obtained. Another problem with lower air distance is the increase in input loss [2].

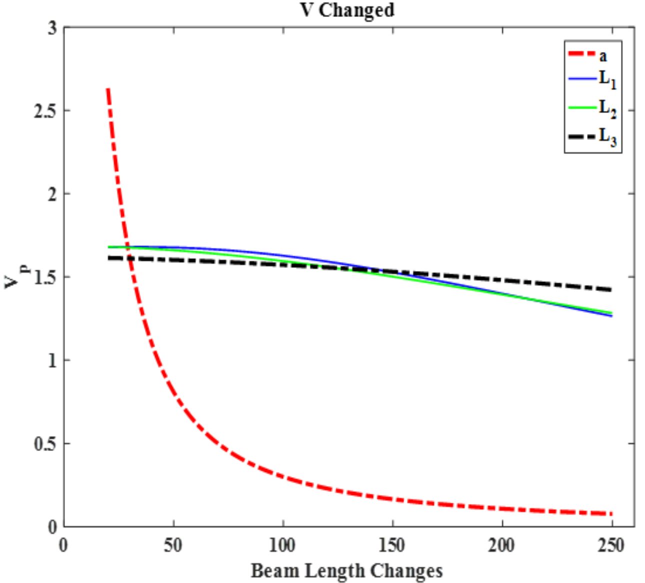

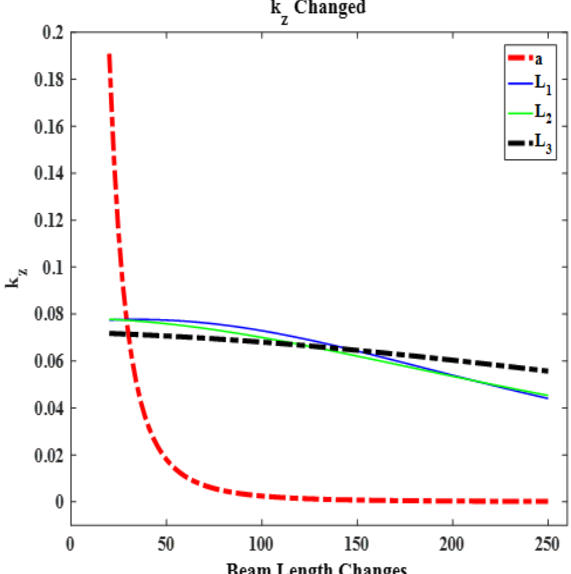

Fig. 3. The effect of different sections of the suggested structure on spring constant (a); The effect of changing different sections of the suggested structure on V_{AC} (b).

TABLE 3: SUMMARY OF THE EFFECT OF STRUCTURE CHANGE ON SPRING CONSTANT AND V_{AC}

Change range (20-250 µm)	Spring constant (N.m^{-1})	V_{AC}(V)
a	0.19-0.01	2.6-0.5
L_1	0.079-0.045	1.6-1.4
L_2	0.079-0.048	1.6-1.4
L_3	0.076-0.065	1.55-1.5

B. V_{AC} Calculation

Recently, researchers have used all three ways to reduce V_{AC}. Structure design with a low spring constant is the best method [18-20]. In order to decrease V_{AC} in the designed switch, a spring constant reduction method with non-uniform curves is used, and the replacement of a designed switch by voltage exertion in COMSOL software is demonstrated in Fig . 4(a). In this Fig ., switching is performed by replacing approximately 1/3 of the air distance [2].

The designed switch needs 1.8 V of actuation voltage for switching. Fig . 4(b) shows the simulation result in COMSOL software. For the simulation,thefirst mobile section and dielectric are illustrated. Then,a 2.5 µm air distance is applied between the mobile section and the fixed section. Finally, the mobile section is made up of gold and dielectric, and silicon nitride was utilized in the simulation. Actuation is electrostatically applied to the mobile section, and the ground is considered as the border between dialectic and air distance.

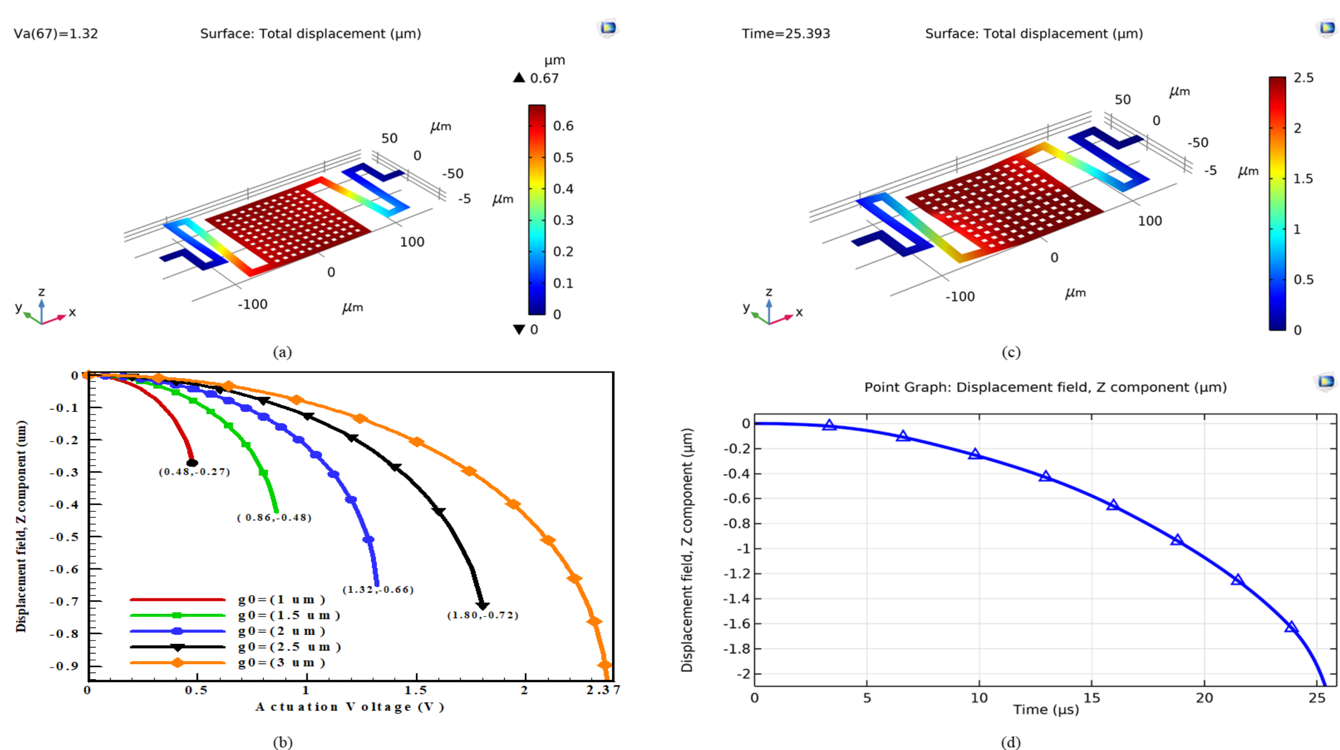

Fig. 4. Suggested switch replacement based on the electrostatic actuation (a); The V_{AC} for the designed switch (b); switching time of the designed switch (c); Replacement in switching time (d).

TABLE 4: COMPARISON BETWEEN MODEL AND SIMULATION V_{AC} VALUE VERSUS DIFFERENT AIR DISTANCES FOR THE SUGGESTED STRCTURE.

Air distance (µm)	Model V_{AC} (V)	Simulated V_{AC} (V)	Error (%)
1.0	0.41	0.48	14.0
1.5	0.75	0.86	12.0
2.0	1.15	1.32	12.0
2.5	1.61	1.80	10.0
3.0	2.12	2.37	10.0

C. Switching Time

Switching and RF-MEMS speed is less than semi-conductive and PIN diode and it is one of the limitations of RF-MEMS switches. Damping, mass, switch structure, and spring constant value impact the switching time. Using materials such as $ALSI_{0.04}$ with smaller mass may enhance switching speed [13] and other reported literature (see Table 6). Fig . 4(c)

shows the result of the switching time simulation for the designed structure in COMSOL software, which is 25.3 μs for this structure. Fig . 4(d) shows the movement in the whole air distance. The next section is dedicated to the calculation of mass and switch natural frequencies which greatly influence the switch function.

D. Natural Frequencies and the Designed Switch Mass

Switch natural frequencies and switch mass influence switch spring constant and finally V_{AC} such that the less the switch mass, the more the switching speed. Also, high natural frequencies enhance V_{AC} and reduce switching time. Thus, the switch is designed in a way that this negligence is considered [22]. Table 5 shows the first six natural frequencies of the designed switch and themass related to switching. The determination of the resonance frequency value is governed by the following relationship:

$$f_0 = \frac{1}{2*\pi}\sqrt{\frac{k}{m}} \tag{16}$$

In this equation, "k" represents the spring constant, and "m" signifies the effective mass of the cantilever beam. For the calculations presented in this article, the first mode, which aligns with the movement direction of the switch actuation, has been considered. The mass and spring constant values for the specified structure are determined to be 0.206 ng and 0.079 N $m^{(-1)}$ respectively. Consequently, the value of the first mode is confirmed to be 3118.8 Hz.

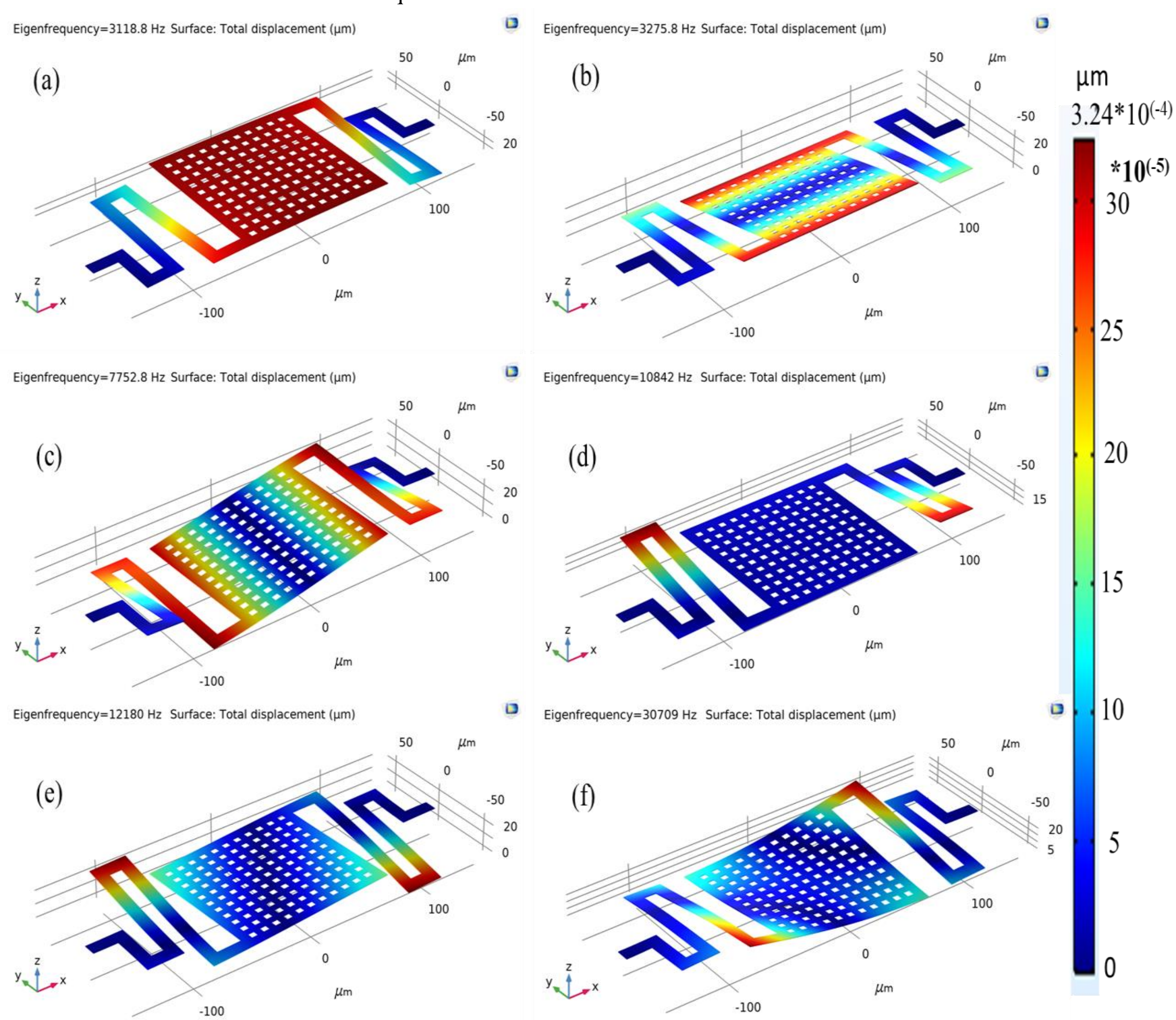

Fig. 5. Designed switch replacement in six natural frequencies, (a): 3118.63 Hz, (b): 3275.60 Hz, (c): 7752.09 Hz, (d): 10842.59 Hz, (e): 12180.50 Hz, (f): 30709.47 Hz

TABLE 5. SIX NATURAL FREQUENCIES OF THE DESIGNED SWITCH (MASS=0.206ng).

Frequency number	Natural frequency
1	3118.63
2	3275.60
3	7752.09
4	10842.59
5	12180.50
6	30709.48

E. Von Mises Stress for the Mechanical Structure

Von Mises Stress is one of the most important issues that must be studied in mechanical analysis, which is measured to guarantee the design safety. Comparing this value with material yield strength defines whether thestructure must be specially designed or not. In fact, if themaximum tolerable stress is more than material strength, the design fails, and if themaximum tolerable stress is less than material strength, the design is safe. For the suggested design, this value is 4.5 MPa, which is shown in Fig . 6, the maximum value obtained for silicon ground is within the acceptable range.

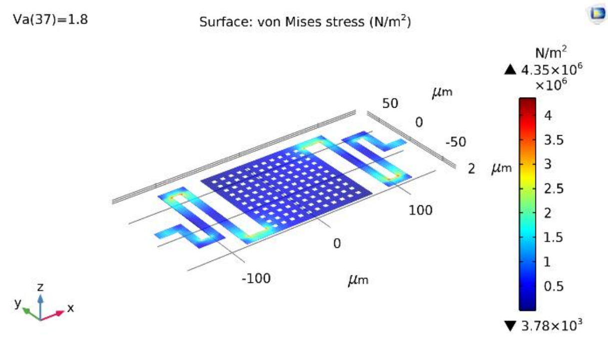

Fig. 6. Von Mises Stress for the suggested structure.

F. Spring Constant Value based on Simulation Results

A replacement proportionate to 1/3 of the air distance is necessary for the switch to function properly [1]. Hence, $g = \frac{2}{3} g_0$. On the one hand, according to Eq. 16, spring constant for the suggested structure is 0.075 N m^{-1}.

$$K = m * \ (2\pi f_1)^2 = (206 * 10^{-9}) * (2 * \pi * 3118.6)^2 \ = 0.079$$

(17)

G. RF Performance

Traditional capacitive RF MEMS switches consist of a coplanar waveguide (CPW) connected to a transmission line, a floating membrane serving as an actuator, and an electrode for applying a bias voltage. This bias voltage enables the switch to transition between its on and off states. The up-state capacitance (C_u), down-state capacitance (C_d), and capacitive ratio (C_r) can be computed as follows:

$$C_r = \frac{C_d}{C_u} = \frac{\frac{\varepsilon_0 \varepsilon_r A}{t_d}}{\frac{\varepsilon_0 A}{g + \frac{t_d}{\varepsilon_r}} + C_f} = \frac{g_0 \varepsilon_r}{t_d} + 1 \qquad (18)$$

A higher C_r indicates superior RF performance. To evaluate and enhance the RF performance, simulations were conducted using HFSS software. The RF performance is characterized by S parameters, which can be obtained as follows [21]:

$$S_{11} = -20 \, log \left| \frac{-Z_h}{2Z_h + Z_0} \right| \qquad (19)$$

$$S_{21} = -20 \, log \left| \frac{2Z_h}{2Z_h + Z_0} \right| \qquad (20)$$

The parameters Z_0 and Z_h represent the CPW impedance and cantilever beam impedance, respectively. The evaluation of RF performance involves defining return loss, insertion loss, and isolation. Isolation is defined as the ratio of transmitted power to submitted power in the down state, where a higher isolation indicates better RF performance. S_{12} signifies the isolation at the down state and insertion loss at the up state, while S_{11} represents the return loss at both the down and up states. In Fig. 7, the switch diagram is illustrated, and Fig. 8 depicts the simulated results for S_{11} and S_{12}, respectively. Simulation results indicate that the return loss is better than -1 dB at 46 GHz in the up state, and it remains more than -10 dB from 40 GHz to 50 GHz in the down state. The insertion loss is better than -0.7 dB at 46 GHz, and the isolation exceeds -25 dB from 40 GHz to 35 GHz with an actuation voltage of 1.8 V. Notably, the maximum isolation achieved is -29 dB at 46 GHz. These results highlight the favorable RF performance of the switch.

In this paper, the switch is based on silicon and a 0.15 µm-thich Si_3N_4 dielectric material is used. The CPW line has a size of 56/120/56 (G/S/G) µm and the size of the beam is 120 µm width and 300 µm length.

H. fabrication

The fabrication of the MEMS switch entails the utilization of a high-resistance silicon substrate, wherein successive layers of SiO_2, Si_3N_4, and Au are deposited. The manufacturing process encompasses photolithography, electron beam evaporation, sputtering, and electroplating techniques to fabricate the essential components. Notably, a sacrificial polyimide layer is strategically employed and subsequently eliminated to conclude the switch fabrication process[6].

The fabrication process of the MEMS switch is shown in Fig. 9. The switch is fabricated on 250 µm thickness high-resistance silicon, and a layer of SiO_2 is located above it. Furthermore, photolithograph negative glue was used to photoetching DC bias lines pattern, electron beam evaporation C_r DC bias lines, then stripped photolithograph negative glue, and 0.15 µm-thickness Si_3N_4 is deposited on top of the bias lines. Au layer of 0.3 µm thickness, as CPW lines, is sputtered on the substrate, and a layer of Si_3N_4 is located on the top of

the transmission lines as a dielectric layer. A 2 μm-thick polyimide is used as the sacrificial layer after the thermal curing process. The 0.6 μm-thick anchors and beams are formed by electroplating technology. The sacrificial layer is released using supercritical dry release[8, 22].

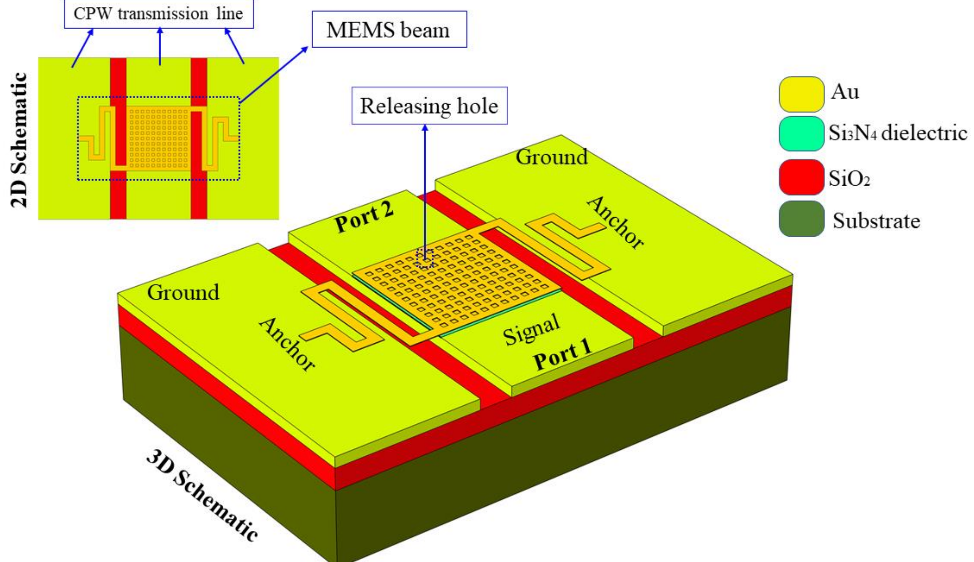

Fig.7. Schematic view of the structures of the RF MEMS switch.

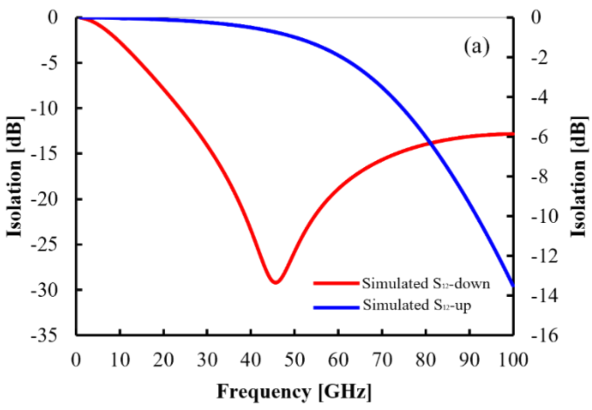

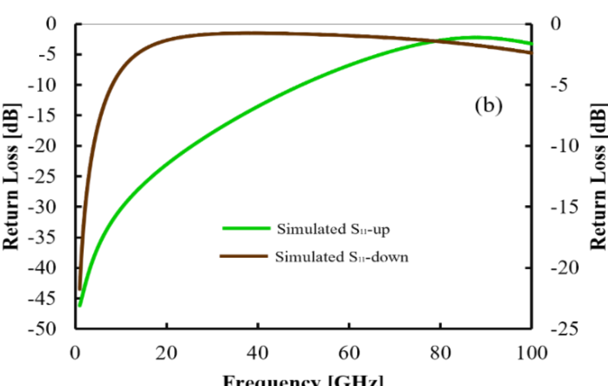

Fig.8. (a) S_{12} of the simulated results; (b) S_{11} of the simulated results

I. Conclusions

In this research, a novel architecture for radiofrequency microelectromechanical system (RF-MEMS) switches based on new numerical and simulation analyzing approaches. For the proposed RF-MEMS the spring constant (*k*) as the key characteristic mechanical parameter was analyzed for RF-MEMSs using the modified energy method (MEM). The proposed architecture provided ahighly flexible structure with low actuation voltage (V_{AC}) based on gold (Au) and silicon nitride (Si_3N_4) as the reticular beam and the dielectric layer, respectively. The COMSOL package was applied for analyze and simulate the structure from themechanical point of the view and the findings confirmed that the altering in position and length (L) values of beams not only diminishes the *k* outstandingly but also provides an ultra-sensitivity for V_{AC} and great concomitance between numerical and simulation *k* and V_{AC} values as well. The V_{AC} value for the L-dependent numerical *k* was obtained at1.61 V which closely was validated with simulation outputs that were at 0.08 N m^{-1} and 1.80 V, respectively. Additionally, the switching time (t_s), Von Mises Stress (VMS), natural frequency (f_n) and mass (m) have been introduced as the key characteristic mechanical parameters with values about 25.60 μs, 4.50 MPa, 3118.60 Hz , , and0.21 ng, respectively that could play significant cooperative factors. The results confirm that the return loss remains below -1 dB at 46 GHz during both the ON and OFF states and exceeds -10 dB from 40 GHz to 50 GHz. This study introduces a novel perspective into the design and application paradigm for trials targeting low actuation voltage (V_{AC}) for RF-MEMS switches. Compared with other capacitive RF-MEMS switch , as shown in Table 6.

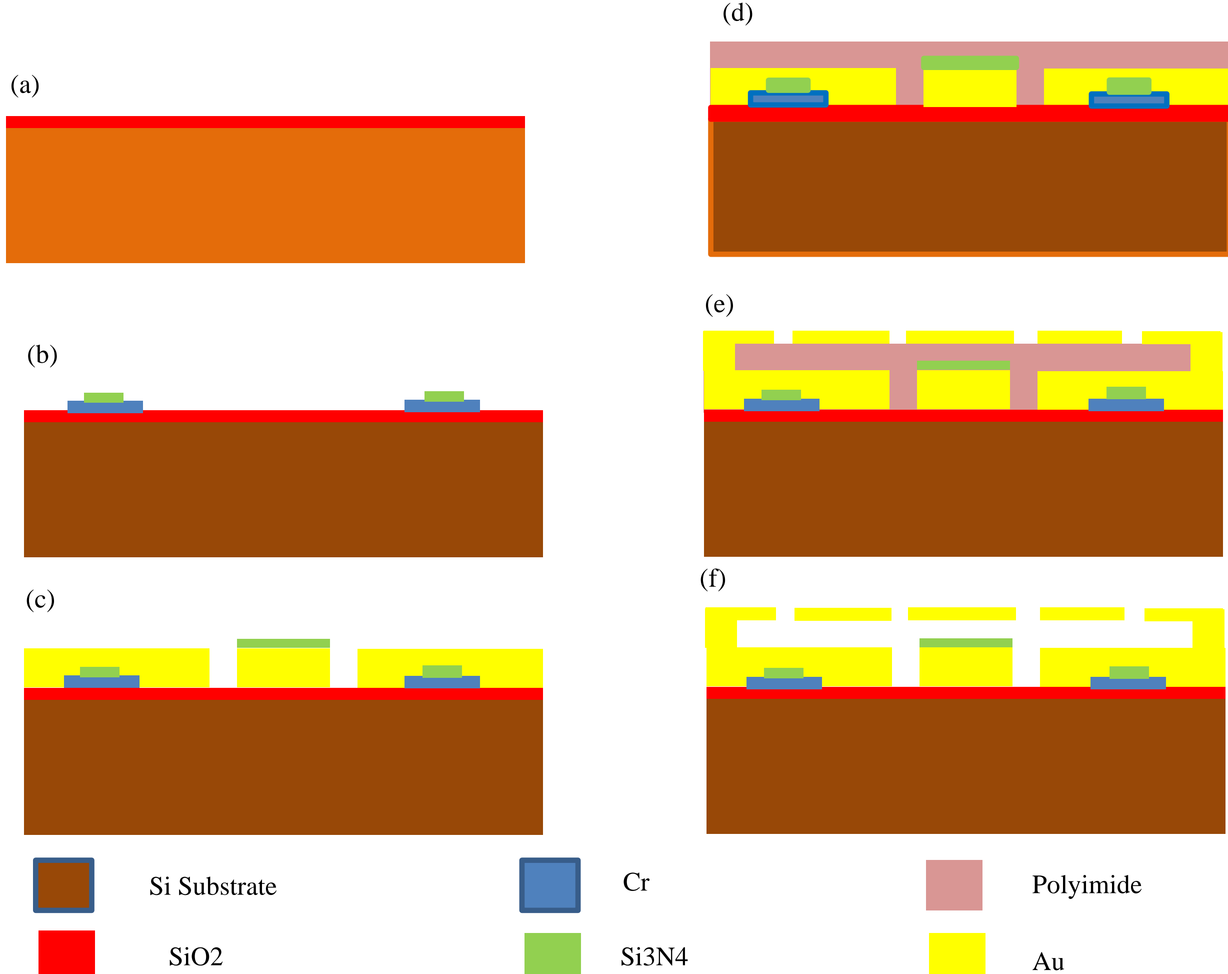

Fig. 9. The device fabrication process: (a) Silicon substrate post-oxidation; (b) Creation of high-resistance direct current (DC)-bias line and patterning of the Si3N4 dielectric layer; (c) Patterning of coplanar waveguide (CPW) lines; (d) Application of polyimide spinning to generate a sacrificial layer followed by chemical mechanical polishing (CMP) to diminish surface roughness of polyimide; (e) Patterning of gold layer to construct MEMS beams and anchors; (f) Removal of the sacrificial layer[8, 22].

TABLE 6: COMPARISON MECHANICAL PARAMETER OF PROPOSED SWITCH WITH PREVIOUS REPORTS

Ref.	Actuation mechanism	Beam material (μm)	Air gap (μm)	Dielectric material (μm)	Actuation voltage(V)	Switching time(μs)	Von Mises Stress
[22]	Electrostatic	1.60(Au)	2.00	(Si_3N_4)	4.40	22	18 MPa
[23]	Electrostatic	0.50	2.00	0.15 (Si_3N_4)	2.64	25.40	N/A
[24]	Electrostatic	0.50	2.00	0.10 (SiO_2)	1.80	11.20	N/A
[19]	Electrostatic	1.20 (Au)	3.70	1.00 (Si_3N_4)	10.60	N/A	41.70 MPa
[25]	Electrostatic	0.50 (Au)	3.00	(HfO_2)	2.40	96.00	N/A
[26]	Electrostatic	1.50 (Au)	2.00	1.50 (Si_3N_4)	3.30	N/A	N/A
[27]	Electrostatic	1.60 (Au)	N/A	0.10 (Si_3N_4)	2.54	N/A	N/A
[13]	Electrostatic	0.60 (Au)	2.50	0.15 (Si_3N_4)	2.10	58.72	N/A
Proposed switch	**Electrostatic**	**0.60 (Au)**	**2.5/2**	**0.15 (Si_3N_4)**	**1.80/1.15**	**25.60**	**4.50 MPa**

References

[1] B. Bakeer, A. Elsabbagh, and M. Hedaya, "Parametric optimization of non-prismatic micro-plates to reduce stiffening and curling initiated during fabrication," in *IOP Conference Series: Materials Science and Engineering*, 2021, vol. 1172, no. 1: IOP Publishing, p. 012021.

[2] G. M. Rebeiz, *RF MEMS: theory, design, and technology*. John Wiley & Sons, 2004.

[3] H. R. Ansari, S. Khosroabadi, and Y. Mafinejad, "Design and simulation of a RF MEMS shunt capacitive switch with low actuation voltage, low loss and high isolation," *Journal of Iranian Association of Electrical and Electronics Engineers,* vol. 18, no. 1, pp. 29-35, 2021.

[4] F. Khan and M. I. Younis, "RF MEMS electrostatically actuated tunable capacitors and their applications: a review," *Journal of Micromechanics and Microengineering,* vol. 32, no. 1, p. 013002, 2021.

[5] A. S. Khan and T. Shanmuganantham, "Arc-shaped cantilever beam RF MEMS switch for low actuation voltage," in *2017 IEEE International Conference on Circuits and Systems (ICCS)*, 2017: IEEE, pp. 302-305.

[6] K. Han, Y. Liu, X. Guo, Z. Jiang, N. Ye, and P. Wang, "Design, analysis and fabrication of the CPW resonator loaded by DGS and MEMS capacitors," *Journal of Micromechanics and Microengineering,* vol. 31, no. 6, p. 065004, 2021.

[7] N. Habbachi and K. Besbes, "RF MEMS filter based on dual liquid variations," *Journal of Micromechanics and Microengineering,* vol. 32, no. 6, p. 065002, 2022.

[8] K. Deng, F. Yang, Y. Wang, C. Lai, and K. Han, "Design and Fabrication of a Ka Band RF MEMS Switch with High Capacitance Ratio and Low Actuation Voltage," *Micromachines,* vol. 13, no. 1, p. 37, 2022.

[9] J. Li, Z. Chen, W. Liu, J. Yang, Y. Zhu, and F. Yang, "A novel piezoelectric RF-MEMS resonator with enhanced quality factor," *Journal of Micromechanics and Microengineering,* vol. 32, no. 3, p. 035002, 2022.

[10] A. K. Sharma and N. Gupta, "Investigation of actuation voltage for non-uniform serpentine flexure design of RF-MEMS switch," *Microsystem technologies,* vol. 20, no. 3, pp. 413-418, 2014.

[11] K. Khodadady and B. A. Ganji, "Design and modeling of a novel RF MEMS series switch with low actuation voltage," *Microsystem Technologies,* vol. 22, no. 12, pp. 2921-2929, 2016.

[12] N. Van Der Meijs and J. Fokkema, "VLSI circuit reconstruction from mask topology," *Integration,* vol. 2, no. 2, pp. 85-119, 1984.

[13] K. Guha, N. Laskar, H. Gogoi, K. Baishnab, and K. S. Rao, "A new analytical model for switching time of a perforated MEMS switch," *Microsystem Technologies,* vol. 26, no. 10, pp. 3143-3152, 2020.

[14] K. Guha, N. Laskar, H. Gogoi, A. Borah, K. Baishnab, and S. Baishya, "Novel analytical model for optimizing the pull-in voltage in a flexured MEMS switch incorporating beam perforation effect," *Solid-State Electronics,* vol. 137, pp. 85-94, 2017.

[15] Y. Mafinejad, A. Kouzani, K. Mafinezhad, and R. Hosseinnezhad, "Low insertion loss and high isolation capacitive RF MEMS switch with low pull-in voltage," *The International Journal of Advanced Manufacturing Technology,* vol. 93, no. 1, pp. 661-670, 2017.

[16] F. P. Beer, E. Johnston Jr, M. Russell, F. David, and E. R. Eisenberg, "Vector Mechanics for Engineers: Statics (SI Units)," *McGraw Hill Higher Education, 9th Revised edition (October 2010), Capítulo,* vol. 3, p. 75, 2019.

[17] F. Khamoii Toli and J. Yavand Hasani, "Design, simulation and optimization of an RF MEMS capacitive switch to reduce actuation voltage," *Journal of Iranian Association of Electrical and Electronics Engineers,* vol. 19, no. 2, pp. 1-11, 2022.

[18] V. K. Varadan, K. J. Vinoy, and K. A. Jose, *RF MEMS and their applications*. John Wiley & Sons, 2003.

[19] K. G. Sravani *et al.*, "Designing of RF-MEMS Capacitive Contact Shunt Switch and Its Simulation for S-band Application," in *Micro and Nanoelectronics Devices, Circuits and Systems*: Springer, 2022, pp. 439-448.

[20] A. Tkachenko, I. Lysenko, M. Denisenko, and O. Ezhova, "Design and Optimization of a Shunt RF MEMS Switch with a Hybrid Contact Type," in *International Youth Conference on Electronics, Telecommunications and Information Technologies*, 2022: Springer, pp. 281-299.

[21] A. Tkachenko, I. Lysenko, and A. Kovalev, "Investigation and Research of High-Performance RF MEMS Switches for Use in the 5G RF Front-End Modules," *Micromachines,* vol. 14, no. 2, p. 477, 2023.

[22] Z. Deng, C. Lai, J. Zhou, and Y. Wang, "Design and analysis of a novel low RF MEMS switch with low pull-in voltage and high capacitance ratio," *Microsystem Technologies,* pp. 1-13, 2023.

[23] M. Gaikwad, N. Deshmukh, and V. Sawant, "Electromagnetic Modelling and Parameters Extraction of Metal Contact and Capacitive Type RF MEMS Switch," in *Artificial Intelligence and Sustainable Computing*: Springer, 2022, pp. 143-153.

[24] P. Ashok Kumar, S. R. Karumuri, G. S. Kondavitee, and K. Guha, "Design and performance analysis of a low-pull-in-voltage RF MEMS shunt switch for millimeter-wave therapy, IoT, and 5G applications," *Journal of Computational Electronics,* pp. 1-8, 2022.

[25] L. N. Thalluri, M. K. Reddy, S. R. Hussain, G. C. Reddy, S. Kiran, and K. Guha, "Iterative Approach for Low Actuation Voltage RF MEMS Switch," in *Micro and Nanoelectronics Devices, Circuits and Systems*: Springer, 2022, pp. 117-128.

[26] K. S. Rao *et al.*, "Design and analysis of RF MEMS shunt switch for V-band applications," *Microsystem Technologies,* pp. 1-8, 2022.

[27] Y. Liu, K. Han, Z. Jiang, N. Ye, and P. Wang, "A High Capacitive Ratio and Low Actuation Voltage RF MEMS Switch for Multi Band: Design and Performance Analysis," in *2021 9th International Conference on Communications and Broadband Networking*, 2021, pp. 305-309.

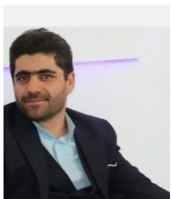

Farid Khamouei Touli was born in Urmia, Iran, in 1990. He received his B.S. and his M.S. degree in Electronics Engineering from Urmia University of Technology, Urmia and Iran University of Science and Technology (IUST),Tehran, Iran, in 2015 and 2019 respectively. He is now an Ph.D. candidate in electrical engineering at Iran University of Science and Technology(IUST),Tehran, Iran. His research interests include Micro-fabrication, RF-MEMS Swithes, Charge Accumulation and Reliability Issue in RF MEMS. He focus on the modeling, design and fabrication of RF-MEMS passive components for 5G& 6G internet.

Dr. Javad Yavand Hasani is a professor in the School of Electrical Engineering at Iran University of Science and Technology (IUST), Tehran, Iran. In 2009 he received the PhD degree in electrical engineering from the University of Tehran and the PhD degree in high frequency and optics from the University of Joseph Fourier (UJF), Grenoble, France. From 2012–2014 he was the dean of the Electronic Research Center (ERC) in IUST. His current research interests include high frequency circuits and systems, as well as micro-fabrication theory and technology for RF and microwave devices, MEMS and NEMS..